JOURNAL OF MATERIALS SCIENCE 29 (1994) 2847–2859

Optical and ultrasonic properties of europium phosphate glasses

H. M. FAROK, H. B. SENIN, G. A. SAUNDERS
School of Physics, University of Bath, Claverton Down, Bath BA2 7AY, UK
W. POON, H. VASS
Department of Physics, The University of Edinburgh, James Clark Maxwell Building, Kings Buildings, Mayfield Road, Edinburgh EH9 3JZ, UK

To provide an overall picture of the vibrational properties of phosphate glasses containing high concentrations of europium, measurements have been made of their ultrasonic wave velocities and attenuation, optical absorption spectra and laser-induced fluorescence. To examine their valence state, the fluorescence of the glasses has been examined. The spectra do not show any obvious sign of divalent europium ions, only trivalent europium ion fluorescence being observed. Room-temperature absorption spectra of these glasses also provide evidence of only the absorption bands of trivalent europium. The elastic stiffnesses C_{11} and C_{44} continue to increase down to low temperatures and the ultrasonic attenuation is characterized by a broad peak, properties which are consistent with thermally activated relaxations of two-level systems. The longitudinal and shear ultrasonic wave velocities decrease under pressure; the hydrostatic pressure derivatives $(\partial C_{11}/\partial P)_{T,P=0}$ and $(\partial C_{44}/\partial P)_{T,P=0}$ of the elastic stiffness tensor components C_{IJ} and $(\partial B/\partial P)_{T,P=0}$ of the bulk modulus, B_0, are negative. When compressed, the europium phosphate glasses, like their samarium analogues, show the interesting property of becoming easier to squeeze. Measurements, using a pulse superposition technique, of the effect of uniaxial stress on ultrasonic wave velocities have been used to determine the temperature dependences of the third-order elastic stiffness tensor components of $(Eu_2O_3)_{0.186}(P_2O_5)_{0.814}$ and $(Eu_2O_3)_{0.20}(P_2O_5)_{0.80}$ glasses between 77 and 400 K. The uniaxial and hydrostatic pressure dependences of the elastic constants quantify the cubic term in the strain Hamiltonian and the vibrational anharmonicity of the long-wavelength phonons of these glasses. The acoustic mode Grüneisen parameters are negative: application of pressure induces a decrease in the long-wavelength acoustic phonon mode frequencies. As the temperature is reduced the pressure-induced mode softening becomes enhanced. The hydrostatic pressure derivative $(\partial C_{11}/\partial P)_{T,P=0}$ is larger than $(\partial C_{44}/\partial P)_{T,P=0}$ over the whole temperature range, and the longitudinal acoustic mode Grüneisen parameter $|\gamma_L|$ is larger than that $|\gamma_S|$ of the shear wave: the longitudinal mode softens more with pressure than the shear mode. Murnaghan's equation-of-state is used to determine the compression $V(P)/V_0$.

1. Introduction

Phosphate glasses containing rare-earth ions as network modifiers have important applications in laser and optoelectronics technology. Many rare-earth phosphate glasses fluoresce strongly. Glasses containing Eu^{3+} ions are amongst those which can exhibit enduring photoinduced property changes, a particularly interesting and useful feature. Persistent, but erasable, modifications of refractive index have been induced in Eu^{3+} and Pr^{3+} -doped multicomponent oxide glasses subsequent to resonant excitation of certain 4f–4f transitions [1–5]. Permanent refractive index grating formation has been observed in a rare-earth phosphate glass of composition $(Eu_2O_3)_{0.125}(La_2O_3)_{0.125}(P_2O_5)_{0.75}$ at 300 K following excitation of the $^5D_2$ state of Eu^{3+}, using four-wave mixing; a transient grating effect was also found in $(Eu_2O_3)_{0.167}(P_2O_5)_{0.835}$ [6]. It has been suggested that a light-induced reordering of the ligand ions surrounding the rare-earth ion, mediated by high-energy phonons created during the non-radiative relaxation of the excited state, may be responsible for the permanent change in refractive index. A double-minimum potential well model including two possible configurations in the local environment of the Eu^{3+} ions in which the phonons induce transitions between the two wells, was used to account for the effects [3]. These observations have prompted the present study of the optical and ultrasonic properties of europium phosphate glasses: ultrasonic interactions provide a powerful tool for investigation of two-level systems in glasses. Interpretation of the ulrasonic effects requires knowledge of the vibrational and electronic behaviour of these glasses, and so optical absorption,

0022–2461

laser-induced fluorescence and Raman spectra measurements form an integral part of this investigation.

Ultrasonic studies have shown that phosphate glasses containing high concentrations of samarium ions exhibit anomalous elastic behaviour as a function of temperature and pressure [7–13]. The hydrostatic pressure derivatives $(\partial C_{11}/\partial P)_{T,P=0}$ and $(\partial C_{44}/\partial P)_{T,P=0}$ are negative: the long-wavelength acoustic modes soften under pressure. The samarium phosphate glasses have a negative hydrostatic pressure derivative $(\partial B^S/\partial P)_{T,P=0}$ of the adiabatic bulk modulus, B^S: they become easier to squeeze when subjected to high pressure [7]. In marked contrast, lanthanum phosphate glasses show normal elastic response to pressure [8, 9]. The question arises: is such anomalous elastic behaviour restricted to the samarium phosphate glasses or is it shown by other vitreous phosphates containing high rare-earth ion concentrations? To answer this, the temperature and pressure dependences of the velocities of ultrasonic waves have been measured in europium metaphosphate glasses using the pulse-echo overlap technique. The Raman spectra of samarium, lanthanum [7, 8] and europium [12] phosphate glasses are similar, suggesting structural similarity. The complete difference between the elastic behaviours of samarium and lanthanum phosphate glasses under pressure and as a function of temperature is not likely to be due to gross structural dissimilarities. The physical origins of the anomalous negative values obtained for the hydrostatic pressure derivatives $(\partial C_{11}/\partial P)_{T,P=0}$ and $(\partial C_{44}/\partial P)_{T,P=0}$ of the elastic stiffnesses and $(\partial B/\partial P)_{T,P=0}$ of the bulk modulus and the positive values for the corresponding third order elastic stiffness tensor components (TOEC) combinations and the negative acoustic mode Grüneisen parameters, γ_L and γ_S, of the samarium phosphate glasses remain uncertain. There have been several possible explanations [7, 8, 13]. One suggestion was that pressure-varying, volume-sensitive, mixed valence of the samarium ion could produce the differences between the ultrasonic properties of the samarium and lanthanum phosphate glasses. However, considerable doubt was cast on this possibility as a result of laser fluorescence studies [14] which showed that the divalent samarium ion was not present in sufficient quantities to produce the observed large elastic anomalies. Europium (like samarium) can enter a host in either its divalent ($4f^7 5s^2 - {}^8S_{7/2}$) or trivalent ($4f^6 5s^2 - {}^7F_0$) state, making it necessary to ascertain its valence state. This has been achieved by measuring the optical absorption and fluorescence and comparing them with the spectra reported for divalent [15] and trivalent europium ion in various hosts.

2. Experimental procedure

The europium phosphate glasses were made from laboratory reagent 99.9% purity grades of phosphorus pentoxide, P_2O_5, and europium oxide, Eu_2O_3. The mixed oxides were reacted in quantities of about 50 g by heating for about 1 h at 500 °C in a closed alumina crucible in an electric furnace. The mixture was then melted in a second furnace and held for 1 h at 1400 °C. After stirring, the melt was cast into a preheated (500 °C) steel split mould to make up a glass cylinder of 10 mm long and 14 mm diameter. Following casting, the glass was immediately transferred to an annealing furnace at 500 °C and kept there for 24 h, after which the furnace was switched off and the glasses were left to cool down to room temperature, at a cooling rate of 0.5 °C min^{-1}. The glasses were transparent, pale pink in colour and of optical quality. The density was measured at room temperature by Archimedes' method using toluene as a flotation fluid. Samples were polished to have flat and parallel faces to within 10^{-3} rad and had a thickness of about 5 mm which is well suited for optical and ultrasonic measurements. To carry out the ultrasonic experiments under uniaxial pressure, rectangular parallelpiped specimens were made with dimensions of about 1 cm^3 and the three pairs of faces polished flat and parallel to optical precision to within one wavelength of sodium light.

The compositions of the glass samples were determined by quantitative analysis using a Jeol JXA-8600 M electron probe microanalyser (EPMA) fitted with wavelength dispersive spectrometers (WDS). A pure sample of EuS was used as a standard. The microanalyser was fitted with four double-crystal spectrometers which could be used to analyse the X-ray spectrum of the elements present in the glass. Using this technique, the electron beam could be directed at a relatively small area without destroying the sample. The chemical compositions and the density of the glass samples are given in Table I. The results of this analysis lead to an interesting observation. Although the starting charges were varied from 5–25 mol% Eu_2O_3, the compositions of the end-product glasses each turned out to be similar, quite close to $(Eu_2O_3)_{0.25}(P_2O_5)_{0.75}$, which corresponds to the metaphosphate $Eu(PO_3)_3$. This suggests that the metaphosphate is much the most stable composition in the phosphate glasses modified by a high concentration of europium.

The optical absorption spectra of europium ion, introduced into phosphate glass, were measured using a standard commercial double-beam instrument. The fluorescence spectra were excited with the 514.5 nm green line of an argon ion laser with the sample contained in a cryostat capable of reaching 10 K and with temperature control to $\pm$ 1 K. The laser power used was varied from 50–200 mW depending on the resultant fluorescence intensity in the specified spectral region. The scattered fluorescence at 90° to the laser beam was collected and focused into a triple grating monochromator with slitwidths set to 150 μm resulting in 0.045 nm resolution. The Raman spectrum was determined in the same instrument, but with slitwidths set to 400 μm resulting in lower resolution than the fluorescence measurement.

To examine the region in the neighbourhood of 400 nm for any indications of the Eu^{2+} band [16], fluorescence measurements were also made using an ultraviolet line as the excitation source. To do this, the experiments were made using the 260 nm line in a fluorometer in a 90° configuration. An ultra-violet

TABLE I A comparison between the elastic and non-linear acoustic properties of europium phosphate glasses at room temperature (293 K)

	Composition $(Eu_2O_3)_x(P_2O_5)_{1-x}$				
	$x = 0.186$	$x = 0.200$	$x = 0.208$	$x = 0.218$	$x = 0.252$
Density ($kg\,m^{-3}$)	3182	3204	3215	3260	3438
Longitudinal wave velocity ($m\,s^{-1}$)	4727	4671	4639	4600	4525
Shear wave velocity ($m\,s^{-1}$)	2741	2708	2686	2662	2598
Elastic stiffnesses (GPa)					
C_{11}^S	71.1	69.9	69.2	69.0	70.44
C_{44}^S	23.9	23.5	23.2	23.1	23.2
Elastic moduli (GPa)					
B_0^S	39.2	38.6	38.3	38.2	39.5
E^S	59.6	58.6	57.9	57.7	58.2
Poisson's ratio, σ^S	0.247	0.247	0.248	0.248	0.254
Pressure derivatives					
$(\partial C_{11}/\partial P)_{P=0}$	− 2.94	− 2.97	− 3.21	− 3.35	− 2.05
$(\partial C_{44}/\partial P)_{P=0}$	− 1.06	− 1.39	− 1.51	− 1.56	− 0.99
$(\partial B/\partial P)_{P=0}$	− 1.53	− 1.12	− 1.20	− 1.27	− 0.73
Grüneisen parameters					
γ_L	− 0.98	− 0.99	− 1.05	− 1.09	− 0.74
γ_S	− 1.04	− 1.31	− 1.41	− 1.46	− 1.01
γ^{el}	− 1.02	− 1.20	− 1.29	− 1.34	− 0.92

absorbing filter (Ealing OY10) was used to block all the ultraviolet below 300 nm from passing on to the grating so as to prevent any interference between the resulting spectrum of the glass and the excitation line.

The ultrasonic wave velocity and attenuation were measured simultaneously using pulse echo techniques. Ultrasonic waves of 10–60 MHz frequency were propagated and detected by X-cut or Y-cut quartz transducers for longitudinal and shear waves, respectively. To make measurements at low temperature, transducers were bonded to the sample using Nonaq stopcock grease. Measurements from room temperature down to about 200 K were made with Dow resin 276-V9 forming the acoustic bond. Quick-dry colloidal silver was found to be a suitable bonding agent for shear mode insertion between room temperature and 400 K. The sample was placed in a close-cycle helium cryostat and the temperature was monitored using a temperature sensor. The temperature was recorded to better than $\pm$ 0.1 K. The changes in ultrasonic wave velocity with temperature and hydrostatic pressure were determined by using the pulse echo overlap technique [17], which has a sensitivity of better than 1 part in 10^5.

Hydrostatic pressure was applied in a piston-and-cylinder apparatus with silicone fluid as the pressure-transmitting medium. The pressure was determined from the change in resistance of a precalibrated manganin wire coil in the pressure cell.

All three components of the TOEC for an isotropic solid can be obtained from ultrasonic wave-velocity measurements made under uniaxial pressures [18]; this technique, using an automatic frequency-controlled gated-carrier pulse superposition apparatus capable of measuring changes in ultrasonic wave transit time to better than 1 part in 10^7 [19], has been described previously [18]. To circumvent the requirement of determination of pressure-induced changes in sample dimensions, the "natural velocity", W, technique [20] was employed. The stress dependences of the relative changes in natural velocities of both longitudinal and shear ultrasonic waves were found to be linear up to the maximum uniaxial stress applied of 100 bar cm^{-2}. Hence the slope of the experimental results for the dependence of the natural wave velocity upon uniaxial stress could be used to obtain the value of $[d(\rho_0 W^2)/dP]_{P=0}$ required for calculation of the TOEC using the expressions given elsewhere [18]. The effects of the applied uniaxial stress on ultrasonic wave velocity are small; although the systematic errors in absolute magnitude of the TOEC are quite large, the error in the relative-changes with temperature is much smaller.

3. Optical absorption, fluorescence and Raman spectra of europium phosphate glasses

Fig. 1 shows the absorption spectrum in the range 200–620 nm at room temperature of a glass having

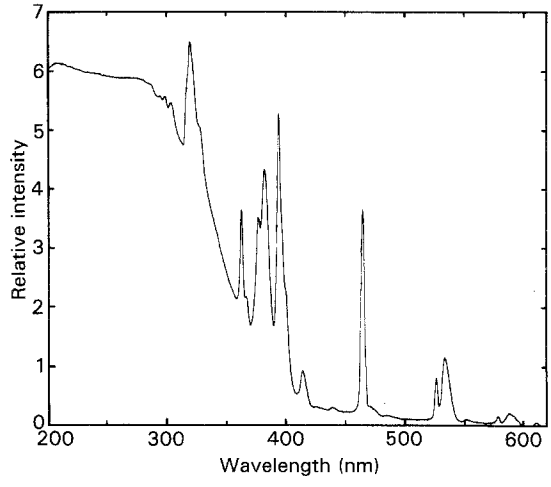

Figure 1 The optical absorption spectrum of a $(Eu_2O_3)_{0.186}(P_2O_5)_{0.814}$ glass at room temperature.

the composition $(Eu_2O_3)_{0.186}(P_2O_5)_{0.814}$. The absorption band peaks are compared in Table II with known data for the Eu^{3+} ion [21]. The band peaks reported for Eu^{3+} ion (column 2) correspond to transitions from the $^7F_0$ ground state and the thermally populated $^7F_1$ to the excited states belonging to the $4f^6$ configuration (column 3). The agreement between the spectral wavelengths (columns 1 and 2) establishes that the bands observed for the $(Eu_2O_3)_{0.186}(P_2O_5)_{0.814}$ glass are typical of Eu^{3+} ion. The absorption bands are sharp; this is usual for those observed for Eu^{3+} and other rare-earth trivalent ions, a characteristic of the small influence of the crystal field on the deep 4f states [22]. Below 400 nm there is strong increase in the background absorption due to the existence of very dense energy levels in this spectral region [23]. This severely limits the resolution of the absorption bands below about 300 nm.

The fluorescence spectrum of $(Eu_2O_3)_{0.186}(P_2O_5)_{0.814}$ glass measured at 300 K resembles that obtained at 10 K but is thermally broadened (Fig. 2). The fluorescence peaks measured at 10 K are compared in Table III with fluorescence lines of Eu^{3+} ion given by Brecher [24]. The close similarity between the two sets of data confirms that this glass contains trivalent europium ions.

However, one aim has been to find out if these glasses contain Eu^{2+} in addition to Eu^{3+}. This can be done by comparing the fluorescence spectrum with that of a material containing a known europium valence state (Table III). For example, the fluorescence of europium-doped $CaSO_4$ consists of a broad band at 385 nm with full-width-at-half maximum of 20 nm and another group of three sharp lines at 597, 625, and 700 nm; the emission in the first group is attributed to Eu^{2+} and the remainder to Eu^{3+} [16]. To find a band in the region of 385 nm in the glass it was necessary to excite using ultraviolet radiation. The fluorescence

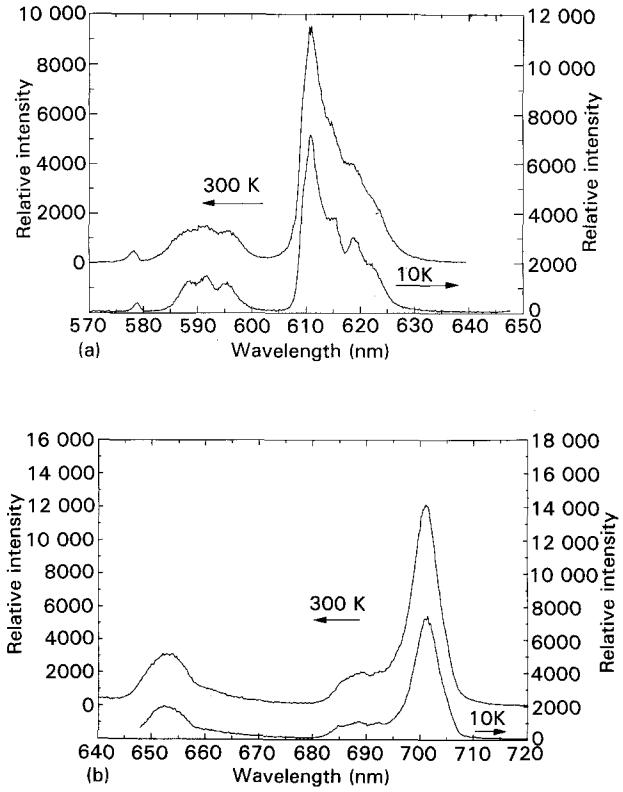

Figure 2 The fluorescence spectra of a $(Eu_2O_3)_{0.186}(P_2O_5)_{0.814}$ glass at 10 and 300 K excited using the green 514.5 nm argon ion laser line. The laser power used to obtain the portion of the spectrum shown in (a) was much less than that for the portion in (b).

TABLE II Measured wavelengths of the absorption bands at room temperature of $(Eu_2O_3)_{0.186}(P_2O_5)_{0.814}$ glass compared with the wavelengths of the absorption bands of Eu^{3+} ion given elsewhere [21]. The transitions which are responsible for these absorption are quoted from the same reference (with the exception of the first two transitions labelled *).

Wavelength (nm) $(Eu_2O_3)_{0.186}(P_2O_5)_{0.814}$ glass	Wavelength (nm) [21]	Transition [21]
610	–	$^5D_0 \leftarrow {}^7F_2^*$
588	–	$^5D_0 \leftarrow {}^7F_1^*$
578	577.5	$^5D_0 \leftarrow {}^7F_0$
534	531.9	$^5D_1 \leftarrow {}^7F_1$
527	526.0	$^5D_1 \leftarrow {}^7F_0$
465	464.5	$^5D_2 \leftarrow {}^7F_0$
415	414.5	$^5D_3 \leftarrow {}^7F_0$
400	399.5	$^5L_6 \leftarrow {}^7F_1$
394	393.4	$^5L_6 \leftarrow {}^7F_0$
382	381.9	$^5L_7 \leftarrow {}^7F_1$
377	378.9	$^5G_2 \leftarrow {}^7F_1$
368	375.2	$^5G_4 \leftarrow {}^7F_0$
363	362.0	$^5D_4 \leftarrow {}^7F_0$
328	–	–
320	–	–

TABLE III Measured wavelengths of the fluorescence band peaks of $(Eu_2O_3)_{0.186}(P_2O_5)_{0.814}$ glass at temperature of 10 K compared with the wavelengths of the fluorescence lines of Eu^{3+} ion in ultraphosphate crystal (EuP_5O_{14}) given elsewhere [24]. The transitions which are responsible for these fluorescences are quoted from the same reference

Wavelength (nm) $(Eu_2O_3)_{0.186}(P_2O_5)_{0.814}$ glass	Wavelength (nm) [24]	Transition [24]
578.8	578.4	$^5D_0 \rightarrow {}^7F_0$
588.3	587.6	$^5D_0 \rightarrow {}^7F_1$
591.4	591.8	
595.1	594.7	
611.0	611.6	$^5D_0 \rightarrow {}^7F_2$
614.7	612.4	
618.5	616.6	
	617.6	
	620.8	
652.1	648.5	$^5D_0 \rightarrow {}^7F_3$
	648.8	
	649.4	
	650.6	
	651.0	
	653.3	
	654.6	
701.3	687.2	$^5D_0 \rightarrow {}^7F_4$
	689.9	
	690.7	
	692.3	
	693.5	
	698.5	
	698.8	
	700.2	
	701.8	

obtained at 45° from the surface of the $(Eu_2O_3)_{0.186}(P_2O_5)_{0.814}$ glass excited using the 260 nm ultraviolet line is shown in Fig. 3. Two distinct spectral regions can be seen. The first one comprises two sharp bands around 600 nm which can definitively be attributed to the Eu^{2+} ion fluorescence [16], although they are not resolved into their components because the resolution of the grating is too low and also the ultraviolet exciting line is broad, unlike the laser line. The second spectral region comprises overlapped bands from 350–550 nm, which are not due to Eu^{2+} ions. This overlapped band originates from the absorption bands (Fig. 1) of the Eu^{3+} acting as fluorescence bands. It is not obtainable in the 90° configuration; in this configuration, when the Eu^{3+} bands are excited, any fluorescence obtained from the absorption bands in the range 350–550 nm is low in intensity and is reabsorbed by Eu^{3+} ions. It is important to note that, as a result of the allowed transition $4f^7 \rightarrow 4f^6 5d$ [25], the absorption bands of the Eu^{2+} ions around 232.7, 322 and 288.5 nm [26] are two orders of magnitude stronger than those of the Eu^{3+} ions, yet they are not shown in the absorption spectrum (Fig. 1): the content of Eu^{2+} ions is minimal.

The first peak in the fluorescence spectrum at 10 K (Fig. 2a) is attributed to the transition $^5D_0 \rightarrow {}^7F_0$ in Eu^{3+} ion. This transition is a singlet because the $^7F_0$ level is non-degenerate ($J = 0$). Trial fits to this peak have been made using a Gaussian distribution routine. A good fit could only be achieved using two Gaussian peaks (Fig. 4b) rather than one (Fig. 4a). The

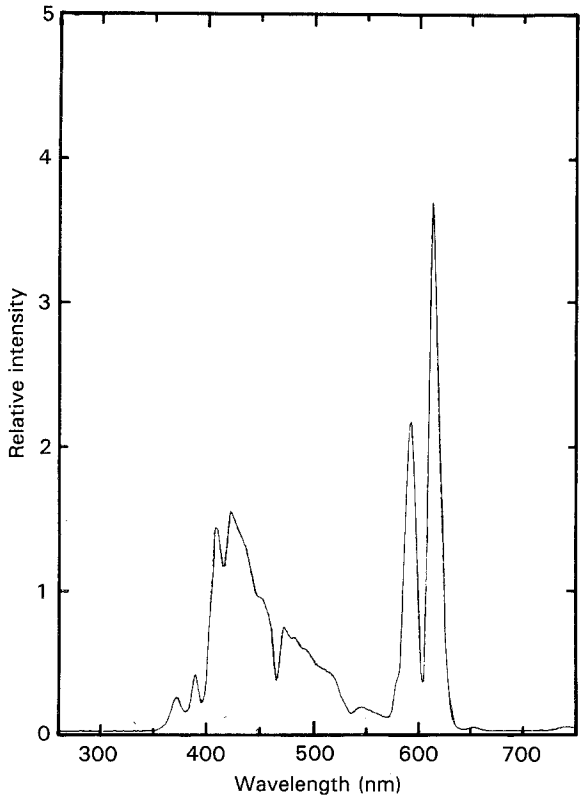

Figure 3 The fluorescence spectrum of a $(Eu_2O_3)_{0.186}(P_2O_5)_{0.814}$ glass at room temperature excited using the ultraviolet 260 nm line. The fluorescence has been collected at a 45° configuration from the surface of the glass.

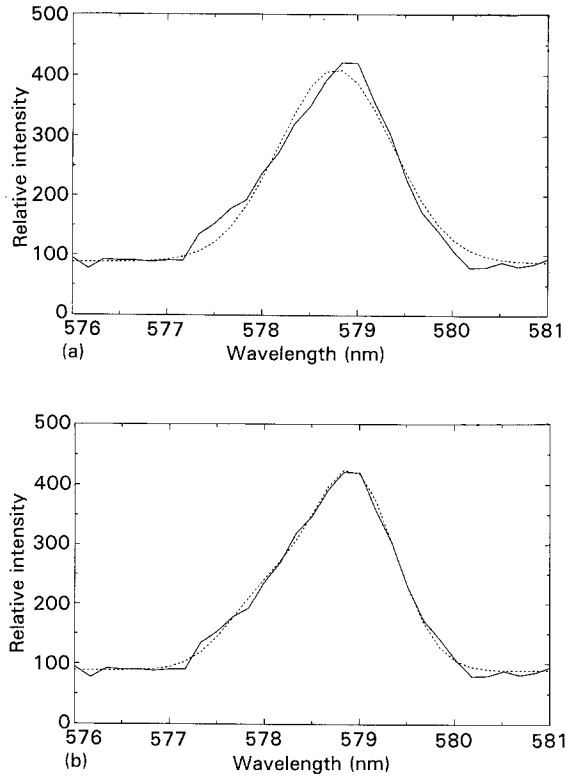

Figure 4 The $^5D_0 \rightarrow {}^7F_0$ transition of $(Eu_2O_3)_{0.186}(P_2O_5)_{0.814}$ glass at 10 K fitted by (a) a single Gaussian distribution ($\chi^2 = 0.12 \times 10^5$) and (b) two Gaussian distributions ($\chi^2 = 0.06 \times 10^5$). (——) Data, (- - -) Gaussian fitting.

wavelengths from this two Gaussian fit are 578 and 578.9 nm, corresponding to an energy difference of $\Delta E = 0.0033$ eV. The $^5D_0 \rightarrow {}^7F_1$ transition of this glass at 10 K has been fitted in the same way. This transition consists of three peaks (Table III and Fig. 2a). However, six Gaussian distributions are needed (Fig. 5b), rather than three (Fig. 5a), to provide a good fit. The wavelength values of the peaks of the six fitted Gaussians are 587.6, 589.2, 590.7, 592.1, 594.4 and 596 nm. The difference in wavelengths between the first two of these peaks corresponds to an energy difference of $\Delta E = 0.0058$ eV; that between the third and the fourth Gaussians results in an energy difference of $\Delta E = 0.0049$ eV and between the fifth and the sixth Gaussians to $\Delta E = 0.0056$ eV. The same procedure has been applied to the transition $^5D_0 \rightarrow {}^7F_2$ which consists of five peaks. The best fit has been obtained with ten Gaussian distributions. The presence of two peaks instead of one in the transition $^5D_0 \rightarrow {}^7F_0$ (in spite of it being a singlet) and six rather than three for $^5D_0 \rightarrow {}^7F_1$ and ten peaks instead of five for $^5D_0 \rightarrow {}^7F_2$ suggests the europium ions are sited in at least two different low-symmetry environments, which are shifted from each other by an energy difference of approximately $\Delta E = 0.0033$ eV, which has been taken because the fit to the singlet transition ($J = 0$) is the most reliable.

The Raman spectrum of $(Eu_2O_3)_{0.186}(P_2O_5)_{0.814}$ glass excited by the 514.5 nm argon ion laser line at 10 and 300 K is shown in Fig. 6. The Raman spectra of rare-earth phosphate glasses are similar to those of other vitreous phosphates containing different

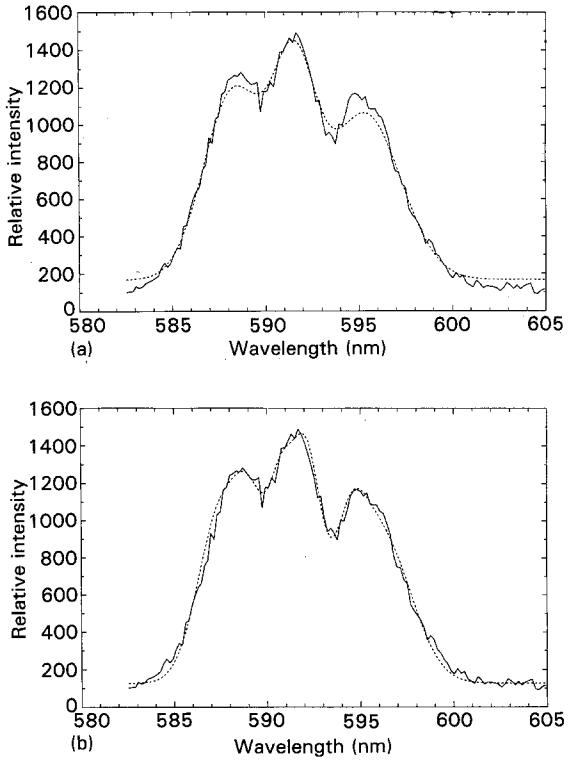

Figure 5 The $^5D_0 \rightarrow {}^7F_1$ transition of $(Eu_2O_3)_{0.186}(P_2O_5)_{0.814}$ glass at 10 K fitted by (a) three Gaussian distributions ($\chi^2 = 0.27 \times 10^6$) and (b) six Gaussian distributions ($\chi^2 = 0.19 \times 10^6$). (——) Data, (- - -) Gaussian fitting.

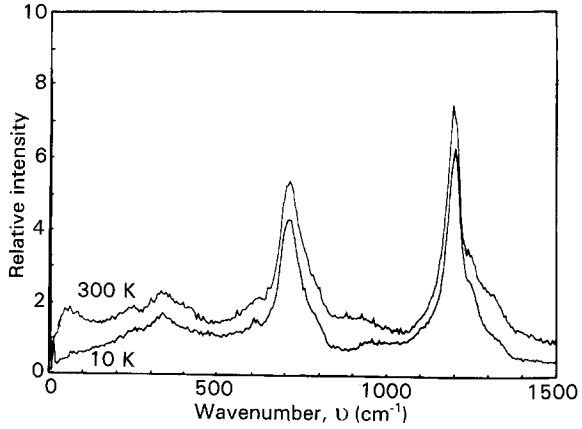

Figure 6 The Raman spectra of $(Eu_2O_3)_{0.186}(P_2O_5)_{0.814}$ glass at 10 and 300 K excited using the green 514.5 nm argon ion laser line.

network modifiers. The phosphate units of these europium glasses must be arranged structurally in a similar way to those in other phosphate glasses. Although there have been no detailed structural investigations of the rare-earth phosphate glasses, there is some pertinent knowledge of the structure of other vitreous phosphates including those formed from alkali oxides [27]. Phosphate glasses are built up from PO_4 tetrahedral units in which one oxygen atom is doubly bonded to the phosphorus and does not contribute to the coherence of the network; pairs of PO_4 tetrahedra can share only one corner. Vitreous P_2O_5 itself is comprised of a three-dimensional disordered network of PO_4 tetrahedra, most of which are linked at three corners. As alkali oxide M_2O is added to the glass-forming oxide P_2O_5, the PO_4 tetrahedra change configuration. As the metal oxide modifier content is increased there is a reduction of the number of cross-linking P–O–P bonds between pairs of tetrahedra and there is a tendency towards an increasing number of chains of PO_4 tetrahedra in the structure. Sodium phosphate glasses having the metaphosphate composition are considered to consist of long polymeric chains comprised of PO_4 tetrahedra connected at two corners so that there are two non-bridging oxygen atoms on each tetrahedron [28, 29]. The infrared spectra of vitreous metaphosphates are consistent with the number of modes available for a zigzag chain rather than for a straight one [30, 31]. In a phosphate glass which is of a composition well below that of a metaphosphate, the structure is a three-dimensional disordered network of PO_4 tetrahedra, most of which are linked at three corners. However, in the vicinity of the metaphosphate composition the chains are linked by the modifier (which in the present case would be Eu^{3+}) cations, which occupy sites between non-bridging oxygen atoms on adjacent chains and provide weaker ionic bonds between the strongly covalently bound chains. The strongest sharp band at about 1195 cm^{-1} is due to symmetric stretching O–P–O vibrations of the non-bridging oxygens relative to the $P–O_{bridging}–P$ which link the PO_4 tetrahedra into polymeric chains. The mode responsible for the strong band near 708 cm^{-1} is a symmetric skeletal stretching vibration of the P–O–P chain linkage [7].

4. Ultrasonic wave velocities, the elastic stiffnesses and their temperature dependences

The velocities of longitudinal, v_L, and shear, v_S, ultrasonic waves, the adiabatic second order elastic stiffness tensor components (SOEC) $C_{11} = \rho v_L^2$ and $C_{44} = \rho v_S^2$ and the bulk modulus B_0^S at room temperature and atmospheric pressure of the series of europium phosphate glasses are presented in Table 1.

The velocities of longitudinal, v_L, and shear, v_S, ultrasonic waves propagated in $(Eu_2O_3)_{0.186}(P_2O_5)_{0.814}$ and $(Eu_2O_3)_{0.20}(P_2O_5)_{0.80}$ glasses have been measured between 10 and 400 K. These data have been used to determine the temperature dependences of the SOEC C_{11} and C_{44} (Fig. 7); they do not conform with the behaviour expected from vibrational anharmonicity, namely a linear increase of the elastic stiffness tensor component with decreasing temperature terminating in a zero slope at low temperatures. The shear stiffness, C_{44}, does increase approximately linearly with decreasing temperature down to about 150 K. However, C_{11} has an anomalous temperature dependence; for the $(Eu_2O_3)_{0.186}(P_2O_5)_{0.814}$ glass it actually decreases with temperature to reach a minimum value at about 180 K; for the $(Eu_2O_3)_{0.20}(P_2O_5)_{0.80}$ glass, C_{11} remains almost independent of temperature from 400 K down to about 160 K. Similar softening has been observed for samarium phosphate glasses [9, 13]. This similarity between the elastic properties of the phosphate glasses, containing high concentrations of

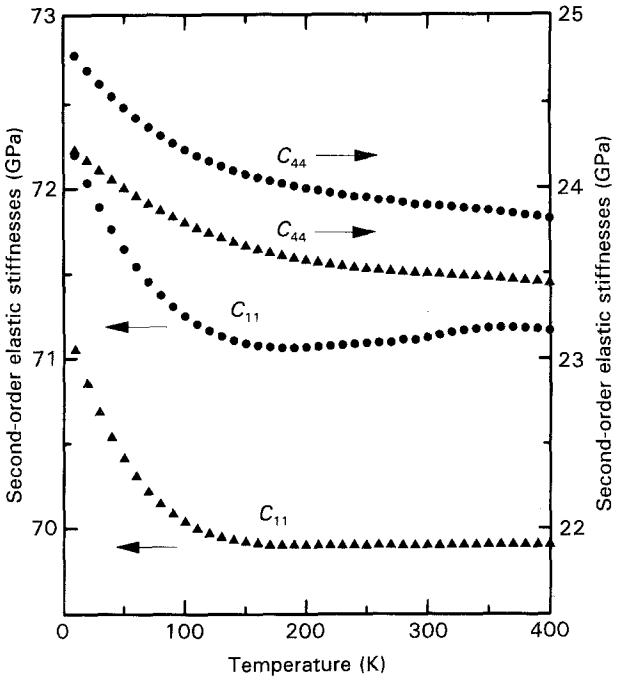

Figure 7 The temperature dependences of the second-order elastic stiffness tensor components C_{IJ} for (●) $(Eu_2O_3)_{0.186}(P_2O_5)_{0.814}$ and (▲) $(Eu_2O_3)_{0.20}(P_2O_5)_{0.80}$ glasses.

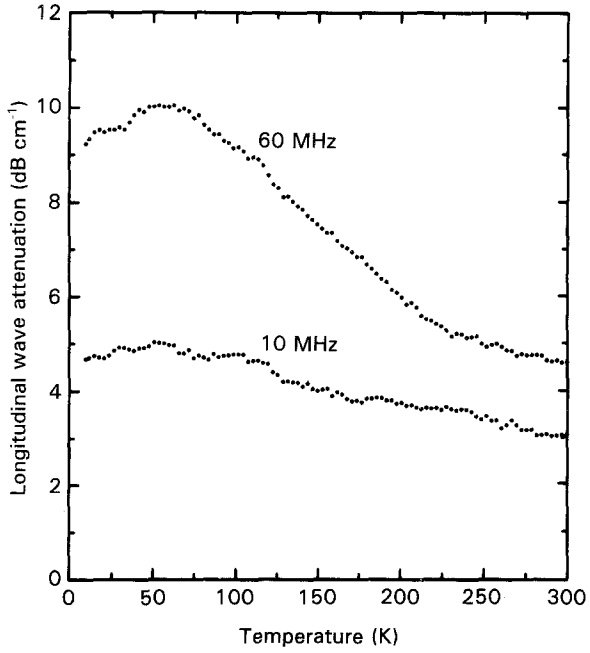

Figure 8 The temperature dependences of the 10 and 60 MHz longitudinal ultrasonic wave attenuation for $(Eu_2O_3)_{0.20}(P_2O_5)_{0.80}$ glass.

samarium or europium, extends down to low temperatures. The velocities of longitudinal, v_L, and shear, v_S, ultrasonic waves propagated in $(Eu_2O_3)_{0.186}(P_2O_5)_{0.814}$ and $(Eu_2O_3)_{0.20}(P_2O_5)_{0.80}$ glasses and hence the elastic stiffnesses, C_{11} and C_{44}, show a continuously steepening increase as the temperature is lowered from about 150 K downwards (Fig. 7). This behaviour is common to many glasses, including vitreous SiO_2 [32–34] and TeO_2 [35]. In vitreous SiO_2 the ultrasonic velocity reaches a maximum at a temperature T_m, below which it decreases as a result of a resonant interaction. Above T_m there is a relaxation effect arising from the energy splitting of the two-level systems in the ultrasonic strain field. The temperatures at which measurements have been made on the europium phosphate glasses should be well above T_m and correspond to the relaxation interaction regime. Evidence for this can be seen in the temperature dependence of the ultrasonic attenuation, which is dominated by a broad peak (Fig. 8) typical of a spectrum of thermally activated relaxations and characteristic of many vitreous materials. Excitations arising from thermally activated motions of relaxing "particles" over potential barriers are believed to be the cause of this broad acoustic attenuation peak.

5. The hydrostatic pressure derivatives of the second order elastic stiffnesses and the third order elastic stiffnesses of europium phosphate glasses

The hydrostatic pressure derivatives $(\partial C_{11}/\partial P)_{P=0}$ and $(\partial C_{44}/\partial P)_{P=0}$ of the elastic stiffnesses and $(\partial B/\partial P)_{P=0}$ of the bulk modulus have been determined at 293 K for the series of europium phosphate glasses (Table I). Each of these pressure derivatives are negative; the SOEC C_{11} and C_{44} soften under pressure, as found for the samarium phosphate glasses [7–13].

The hydrostatic pressure derivative $(\partial B/\partial P)_{P=0}$ of the bulk modulus is negative for each glass (Table I). Hence, the bulk modulus, given to the first-order term in pressure P by

$$B(P) = B_0 + P(\partial B/\partial P) \quad (1)$$

becomes smaller as pressure is increased. Hence these europium phosphate glasses, like the samarium phosphate glasses [7–13], become easier to squeeze under pressure. In contrast, the more usual behaviour under pressure of the elastic stiffnesses is found for vitreous arsenic [36], As_2S_3 [37] and TeO_2 [35] for which $(\partial C_{11}^S/\partial P)_{T,P=0}$, $(\partial C_{44}^S/\partial P)_{T,P=0}$ and $(\partial B^S/\partial P)_{T,P=0}$ are all positive and are almost independent of temperature.

The temperature dependences of the hydrostatic pressure derivatives of the elastic stiffnesses of $(Eu_2O_3)_{0.186}(P_2O_5)_{0.814}$ and $(Eu_2O_3)_{0.20}(P_2O_5)_{0.80}$ glasses between 77 and 400 K are shown in Tables IV and V. As the temperature is reduced to 77 K the anomalously negative values of $(\partial C_{11}/\partial P)_{T,P=0}$ and $(\partial B/\partial P)_{T,P=0}$ becomes much larger. That, $(\partial C_{44}/\partial P)_{T,P=0}$, of the shear modulus also increases but to a much smaller extent. These trends with temperature for $(\partial C_{11}/\partial P)_{T,P=0}$, $(\partial C_{44}/\partial P)_{T,P=0}$ and $(\partial B/\partial P)_{T,P=0}$ are similar to those found for the samarium phosphate glasses [13]. The considerable increases in the negative values of $(\partial B^S/\partial P)_{T,P=0}$ and $(\partial C_{11}^S/\partial P)_{T,P=0}$ of the europium and samarium phosphate glasses shows that the longitudinal acoustic modes soften under pressure and that this softening is considerably enhanced as the temperature is reduced. The derivative $(\partial C_{44}/\partial P)_{T,P=0}$ of the shear modulus is almost independent of temperature.

TABLE IV The hydrostatic pressure derivatives $(\partial C_{IJ}/\partial P)_{T,P=0}$ of the elastic stiffness tensor components and $(\partial B/\partial P)_{T,P=0}$ of the bulk modulus and the acoustic mode Grüneisen parameters of $(Eu_2O_3)_{0.186}(P_2O_5)_{0.814}$ glass as a function of temperature. The errors are: $(\partial C_{11}/\partial P)_{T,P=0}$, ± 0.01; $(\partial C_{44}/\partial P)_{T,P=0}$, ± 0.02; $(\partial B/\partial P)_{T,P=0}$, ± 0.02; γ_L, ± 0.02; γ_S, ± 0.03; γ^{el}, ± 0.03

T(K)	$\left(\frac{\partial C_{11}}{\partial P}\right)_{T,P=0}$	$\left(\frac{\partial C_{44}}{\partial P}\right)_{T,P=0}$	$\left(\frac{\partial B}{\partial P}\right)_{T,P=0}$	γ_L	γ_S	γ^{el}
77	− 10.17	− 1.31	− 8.43	− 2.94	− 1.21	− 1.37
80	− 10.06	− 1.29	− 8.33	− 2.91	− 1.20	− 1.36
90	− 9.59	− 1.29	− 7.88	− 2.79	− 1.20	− 1.34
100	− 9.44	− 1.28	− 7.73	− 2.75	− 1.20	− 1.34
110	− 8.79	− 1.27	− 7.09	− 2.57	− 1.19	− 1.32
120	− 8.34	− 1.27	− 6.65	− 2.45	− 1.19	− 1.30
130	− 8.08	− 1.26	− 6.39	− 2.38	− 1.19	− 1.29
140	− 7.56	− 1.25	− 5.89	− 2.24	− 1.18	− 1.27
150	− 6.93	− 1.24	− 5.27	− 2.07	− 1.17	− 1.25
160	− 6.51	− 1.23	− 4.86	− 1.95	− 1.17	− 1.24
170	− 6.15	− 1.23	− 4.52	− 1.86	− 1.16	− 1.22
180	− 5.79	− 1.21	− 4.18	− 1.76	− 1.15	− 1.20
190	− 5.45	− 1.20	− 3.85	− 1.66	− 1.14	− 1.19
200	− 5.14	− 1.19	− 3.56	− 1.58	− 1.13	− 1.17
210	− 4.73	− 1.18	− 3.16	− 1.47	− 1.13	− 1.16
220	− 4.55	− 1.16	− 3.01	− 1.42	− 1.11	− 1.14
230	− 4.28	− 1.14	− 2.76	− 1.35	− 1.10	− 1.12
240	− 4.06	− 1.13	− 2.55	− 1.28	− 1.09	− 1.11
250	− 3.82	− 1.12	− 2.33	− 1.22	− 1.08	− 1.09
260	− 3.62	− 1.11	− 2.15	− 1.17	− 1.07	− 1.08
270	− 3.44	− 1.09	− 1.99	− 1.12	− 1.06	− 1.07
280	− 3.22	− 1.07	− 1.79	− 1.06	− 1.05	− 1.05
290	− 2.99	− 1.06	− 1.58	− 0.99	− 1.04	− 1.03
293	− 2.94	− 1.06	− 1.53	− 0.98	− 1.04	− 1.02
300	− 2.94	− 1.06	− 1.52	− 0.98	− 1.04	− 1.02
310	− 2.94	− 1.06	− 1.53	− 0.98	− 1.04	− 1.02
320	− 2.95	− 1.06	− 1.53	− 0.98	− 1.04	− 1.02
330	− 2.95	− 1.06	− 1.53	− 0.98	− 1.04	− 1.02
340	− 2.96	− 1.07	− 1.53	− 0.98	− 1.05	− 1.03
350	− 2.95	− 1.07	− 1.53	− 0.98	− 1.05	− 1.03
360	− 2.94	− 1.07	− 1.52	− 0.98	− 1.05	− 1.03
370	− 2.93	− 1.07	− 1.51	− 0.98	− 1.05	− 1.03
380	− 2.92	− 1.07	− 1.49	− 0.97	− 1.05	− 1.02
390	− 2.89	− 1.07	− 1.46	− 0.97	− 1.05	− 1.02
400	− 2.86	− 1.07	− 1.43	− 0.96	− 1.05	− 1.02

For an isotropic material, the cubic terms in the strain Hamiltonian are completely defined by three independent TOEC which can be taken as

$$C_{123} = \nu_1, \quad (2a)$$

$$C_{144} = \nu_2, \quad (2b)$$

$$C_{456} = \nu_3 \quad (2c)$$

The remaining non-zero tensor components are then

$$C_{112} = \nu_1 + 2\nu_2, \quad (3a)$$

$$C_{155} = \nu_2 + 2\nu_3, \quad (3b)$$

$$C_{111} = \nu_1 + 6\nu_2 + 8\nu_3 \quad (3c)$$

The TOEC measured at room temperature for the $(Eu_2O_3)_{0.186}(P_2O_5)_{0.814}$ and $(Eu_2O_3)_{0.20}(P_2O_5)_{0.80}$ glasses are compared with those of other vitreous materials in Table VI. These TOEC, which define the non-linear acoustic properties to third order in strain, tend to be positive in accord with the negative values of $(\partial C_{11}/\partial P)_{T,P=0}$ and $(\partial C_{44}/\partial P)_{T,P=0}$ (the sign of a tensile stress is defined as being positive). The temperature dependences of the TOEC of the $(Eu_2O_3)_{0.186}(P_2O_5)_{0.814}$ glass from 77–400 K are given in Table VII and those for the $(Eu_2O_3)_{0.20}(P_2O_5)_{0.80}$ glass are plotted in Fig. 9.

Both attractive $-B/r^n$ and repulsive A/r^m components of the interatomic potential $\Phi(r)$, which can be represented schematically by

$$\Phi(r) = \frac{A}{r^m} - \frac{B}{r^n} \quad (4)$$

contribute to the elastic moduli. For a glass, which does not have a regular atomic arrangement, r is the mean interatomic distance. The relative contributions depend on the order of the modulus. An adiabatic elastic stiffness tensor component $C_{ijklpq\ldots}$ of order a is the ath derivative $(\partial^a\Phi(r)/\partial\eta_{ij}\partial\eta_{kl}\partial\eta_{pq}\ldots)_{S,\eta=0}$ of the interatomic potential $\Phi(r)$ with respect to Lagrangian strain η_{ij}. For stability the exponent, m must be larger than n, and so the higher the order a, the greater is the influence of the repulsive term A/r^m on the stiffness tensor component $C_{ijklpq\ldots}$ [35]. When a material is subjected to pressure, contraction is resisted by the interatomic repulsive forces, which have a shorter range than the attractive forces and tend to dominate the third-order elastic moduli. Hence the shorter range and large exponent, m, of the repulsive term

TABLE V The hydrostatic pressure derivatives $(\partial C_{IJ}/\partial P)_{T,P=0}$ of the elastic stiffness tensor components and $(\partial B/\partial P)_{T,P=0}$ of the bulk modulus and the acoustic mode Grüneisen parameters of $(Eu_2O_3)_{0.20}(P_2O_5)_{0.80}$ glass as a function of temperature. The errors are: $(\partial C_{11}/\partial P)_{T,P=0}$, ± 0.01; $(\partial C_{44}/\partial P)_{T,P=0}$, ± 0.02; $(\partial B/\partial P)_{T,P=0}$, ± 0.02; γ_L, ± 0.02; γ_S, ± 0.03; γ^{el}, ± 0.03

T(K)	$\left(\frac{\partial C_{11}}{\partial P}\right)_{T,P=0}$	$\left(\frac{\partial C_{44}}{\partial P}\right)_{T,P=0}$	$\left(\frac{\partial B}{\partial P}\right)_{T,P=0}$	γ_L	γ_S	γ^{el}
77	− 10.08	− 1.63	− 7.91	− 2.92	− 1.47	− 1.60
80	− 9.96	− 1.61	− 7.81	− 2.89	− 1.46	− 1.59
90	− 9.51	− 1.61	− 7.37	− 2.76	− 1.46	− 1.57
100	− 9.35	− 1.60	− 7.22	− 2.72	− 1.45	− 1.57
110	− 8.72	− 1.59	− 6.60	− 2.55	− 1.45	− 1.55
120	− 8.28	− 1.59	− 6.16	− 2.43	− 1.45	− 1.53
130	− 8.02	− 1.58	− 5.91	− 2.36	− 1.44	− 1.53
140	− 7.51	− 1.57	− 5.41	− 2.22	− 1.44	− 1.51
150	− 6.89	− 1.56	− 4.81	− 2.06	− 1.43	− 1.49
160	− 6.48	− 1.55	− 4.41	− 1.94	− 1.42	− 1.47
170	− 6.13	− 1.54	− 4.07	− 1.85	− 1.42	− 1.46
180	− 5.77	− 1.53	− 3.74	− 1.75	− 1.41	− 1.44
190	− 5.44	− 1.51	− 3.42	− 1.66	− 1.40	− 1.42
200	− 5.14	− 1.50	− 3.13	− 1.58	− 1.39	− 1.41
210	− 4.73	− 1.49	− 2.74	− 1.47	− 1.39	− 1.39
220	− 4.56	− 1.47	− 2.59	− 1.42	− 1.37	− 1.37
230	− 4.29	− 1.46	− 2.35	− 1.35	− 1.36	− 1.36
240	− 4.07	− 1.44	− 2.14	− 1.29	− 1.35	− 1.34
250	− 3.83	− 1.43	− 1.92	− 1.22	− 1.34	− 1.33
260	− 3.64	− 1.42	− 1.74	− 1.17	− 1.33	− 1.32
270	− 3.46	− 1.41	− 1.58	− 1.12	− 1.32	− 1.30
280	− 3.24	− 1.39	− 1.39	− 1.06	− 1.31	− 1.28
290	− 2.97	− 1.39	− 1.12	− 0.99	− 1.31	− 1.20
300	− 2.98	− 1.38	− 1.12	− 0.99	− 1.30	− 1.19
310	− 2.98	− 1.39	− 1.12	− 0.99	− 1.31	− 1.20
320	− 3.01	− 1.41	− 1.13	− 1.00	− 1.32	− 1.21
330	− 3.06	− 1.42	− 1.17	− 1.01	− 1.33	− 1.22
340	− 3.12	− 1.43	− 1.21	− 1.03	− 1.34	− 1.24
350	− 3.20	− 1.44	− 1.28	− 1.05	− 1.35	− 1.25
360	− 3.29	− 1.44	− 1.38	− 1.08	− 1.35	− 1.26
370	− 3.41	− 1.43	− 1.49	− 1.11	− 1.35	− 1.27
380	− 3.53	− 1.42	− 1.64	− 1.14	− 1.33	− 1.27
390	− 3.67	− 1.39	− 1.82	− 1.18	− 1.31	− 1.27
400	− 3.81	− 1.34	− 2.02	− 1.22	− 1.27	− 1.25

requires predominantly negative of the TOEC, especially $C_{111}(=\partial^3\Phi(r)/\partial^3\eta_{11})$, which is dominated by nearest neighbour repulsive forces and does not have a shear contribution and so should be large and negative. The hydrostatic pressure derivatives of the elastic stiffness tensor components should be positive in a material which shows this normal response to an applied stress. In a glass, the interatomic forces are functions of bond angle as well as atomic separation both of which change under the influence of an applied hydrostatic or uniaxial stress. A complicating feature is that two well systems are present in the amorphous state as a result of the spreads in bond angles and lengths, and the application of pressure perturbs these systems. So far as the effects of pressure (or temperature) on their elastic behaviour are concerned, glasses fall into two distinct categories. Many glasses including amorphous arsenic [36] and As_2S_3 [37], fluorozirconate glass [38] and vitreous TeO_2 [35] behave normally in that the longitudinal, shear and bulk moduli increase under hydrostatic pressure and their TOEC are negative, a feature consistent with the positive signs of the hydrostatic pressure derivatives $(\partial C_{11}/\partial P)_{T,P=0}$, $(\partial C_{44}/\partial P)_{T,P=0}$ and $(\partial B/\partial P)_{T,P=0}$ (Table VI). Phosphate glasses containing the transition elements metals, iron [39] and molybdenum [40], as modifiers also show the normal positive values of the pressure derivatives $(\partial C_{11}/\partial P)_{T,P=0}$ and $(\partial B/\partial P)_{T,P=0}$; as do phosphate glasses containing lanthanum [8, 9] or neodymium [12, 41, 42].

The second-category includes glasses, such as those based on silica [20, 39, 43] and BeF_2 [43], whose non-linear elastic properties are quite different in kind from the majority of materials in that the hydrostatic pressure derivatives $(\partial C_{11}/\partial P)_{T,P=0}$, $(\partial C_{44}/\partial P)_{T,P=0}$ and $(\partial B/\partial P)_{T,P=0}$ are negative and the TOEC are positive. The europium phosphate glasses come into this second category (Tables VI and VII). Application of pressure induces decreases in the elastic stiffnesses of the europium phosphate glasses similar to those observed for the samarium phosphate glasses. The TOEC are mostly positive (Tables VI, VII and Fig. 9). The long-wavelength acoustic modes soften under pressure. For both the $(Eu_2O_3)_{0.186}(P_2O_5)_{0.814}$ and $(Eu_2O_3)_{0.20}(P_2O_5)_{0.80}$ glasses, C_{111}, C_{112}, and C_{123} increase strongly as the temperature is decreased (Table VII and Fig. 9) in a similar way to the TOEC of the samarium phosphate glasses [13] and vitreous SiO_2 [18]. The increase of the TOEC as the temperature is reduced shows that the pressure-induced acoustic mode softening becomes enhanced at lower

TABLE VI The non-linear acoustic properties of $(Eu_2O_3)_{0.186}(P_2O_5)_{0.814}$ and $(Eu_2O_3)_{0.20}(P_2O_5)_{0.80}$ glasses compared with those of other amorphous materials at room temperature (293 K)

	$(Eu_2O_3)_{0.186}(P_2O_5)_{0.814}$ glass	$(Eu_2O_3)_{0.20}(P_2O_5)_{0.80}$ glass	$(Sm_2O_3)_{0.212}(P_2O_5)_{0.798}$ glass [13]	$(Fe_2O_3)_{0.38}(P_2O_5)_{0.62}$ glass [39]	a-As [36]	a-As_2S_3 [37]	Vitreous SiO_2 [18]	Vitreous TeO_2 [35]
C_{111}(GPa)	8	48	− 105	− 450	− 465	− 262	470	− 740
C_{112}(GPa)	74	55	37	− 200	− 33	− 80	234	− 117
C_{123}(GPa)	41	7	10	− 160	− 162	− 26	81	− 185
C_{144}(GPa)	17	24	13	− 18	64	− 27	76	34
C_{155}(GPa)	− 17	− 2	36	− 62	− 108	− 46	59	− 156
C_{456}(GPa)	− 17	− 13	− 25	− 22	− 86	− 9	− 9	− 95
$(\partial C_{11}/\partial P)_{P=0}$	− 2.94	− 2.97	− 1.31	4.52	8.73	9.17	− 9.98	8.61
$(\partial C_{44}/\partial P)_{P=0}$	− 1.06	− 1.36	− 0.67	− 0.16	1.73	1.85	− 2.99	1.65
$(\partial B/\partial P)_{P=0}$	− 1.53	− 1.15	− 0.41	4.73	6.42	6.72	− 5.99	6.41
γ_L	− 0.98	− 0.99	− 0.51	1.1	2.34	2.61	− 2.51	2.28
γ_S	− 1.04	− 1.31	− 0.68	− 0.3	1.45	2.49	− 1.98	1.24
γ^{el}	− 1.02	− 1.20	− 0.67	0.7	1.75	2.53	− 2.05	1.59

temperatures. The hydrostatic pressure derivative $(\partial C_{11}/\partial P)_{P=0}$ is much larger than $(\partial C_{44}/\partial P)_{P=0}$ over the whole temperature range where measurements have been made (Tables IV and V): the longitudinal mode softens more with pressure than the shear mode.

6. The compression $V(P)/V_0$ of europium phosphate glasses

The compression $V(P)/V_0$ of the $(Eu_2O_3)_{0.186}(P_2O_5)_{0.814}$ and $(Eu_2O_3)_{0.20}(P_2O_5)_{0.80}$ glasses at 293 K is compared with those of samarium [13] and neodymium [41, 42] phosphate glass and vitreous SiO_2 [18] in Fig. 10. These compressions have been computed from the ultrasonic velocity and the pressure dependence data using the Murnaghan's equation of state [44, 45]

$$\ln\left(\frac{V_0}{V}\right) = \frac{1}{B_0'}\ln\left[B_0'\left(\frac{P}{B_0^T}\right)+1\right] \quad (5)$$

At comparatively low pressures, the compressions of the phosphate glasses are similar but that for the $(Nd_2O_3)_{0.235}(P_2O_5)_{0.765}$ glass diverges with increasing pressure, due to the fact that this glass has a positive $(\partial B^S/\partial P)_{T,P=0}$ (Table VI).

7. The acoustic mode Grüneisen parameters of europium phosphate glasses

Further physical insight into the vibrational properties of these glasses can be gained by investigating the anharmonicity of their long-wavelength acoustic modes. The longitudinal, γ_L, and shear, γ_S, acoustic mode Grüneisen parameters, which measure the shift $-(\partial \ln \omega/\partial \ln V)$ of the long-wavelength acoustic mode frequency, ω, with volume, V, have been calculated from the second- and third-order elastic stiffness tensor components using

$$\gamma_L = \left[-\frac{1}{6C_{11}}(3B_0 + 2C_{11} + C_{111} + 2C_{112})\right] \quad (6)$$

$$\gamma_S = \left\{-\frac{1}{6C_{44}}\left[3B_0 + 2C_{44} + \frac{1}{2}(C_{111} + C_{123})\right]\right\} \quad (7)$$

For each of the glasses both the longitudinal, γ_L, and shear, γ_S, mode Grüneisen parameters, have negative values at room temperature (Table I): application of pressure leads to a decrease in the mode frequencies, and hence in their vibrational energy. As a result, the mean long-wavelength acoustic mode Grüneisen parameter, γ^{el}

$$\gamma^{el} = \left[\frac{\gamma_L}{v_L^3} + \frac{2\gamma_S}{v_S^3}\right] \Big/ \left[\frac{1}{v_L^3} + \frac{2}{v_S^3}\right] \quad (8)$$

is also negative, intimating that the net contribution from the long-wavelength acoustic phonon modes to the thermal expansion should be negative, but this property remains unexplored for these materials. Above room temperature, the acoustic mode gammas

TABLE VII The third-order elastic stiffness tensor components, C_{IJK} of $(Eu_2O_3)_{0.186}(P_2O_5)_{0.814}$ glass as a function of temperature

T(K)	C_{111} (GPa)	C_{112} (GPa)	C_{123} (GPa)	C_{144} (GPa)	C_{155} (GPa)	C_{456} (GPa)
77	313 ± 15	343 ± 15	290 ± 15	26.4 ± 0.7	− 7.4 ± 0.2	− 16.9 ± 0.5
80	307 ± 15	339 ± 15	288 ± 14	25.8 ± 0.7	− 7.9 ± 0.2	− 16.9 ± 0.5
90	289 ± 15	322 ± 15	270 ± 13	25.5 ± 0.7	− 8.1 ± 0.3	− 16.8 ± 0.5
100	282 ± 15	316 ± 15	265 ± 12	25.3 ± 0.7	− 8.4 ± 0.3	− 16.9 ± 0.5
110	256 ± 14	291 ± 15	241 ± 11	25.0 ± 0.7	− 8.7 ± 0.3	− 16.8 ± 0.5
120	238 ± 13	274 ± 15	224 ± 11	24.9 ± 0.7	− 8.9 ± 0.3	− 16.9 ± 0.5
130	227 ± 12	263 ± 14	214 ± 10	24.7 ± 0.7	− 9.1 ± 0.3	− 16.9 ± 0.5
140	206 ± 10	244 ± 13	196 ± 8	24.4 ± 0.7	− 9.5 ± 0.3	− 16.9 ± 0.5
150	181 ± 8	220 ± 11	172 ± 8	24.1 ± 0.7	− 9.8 ± 0.3	− 16.9 ± 0.5
160	163 ± 7	204 ± 10	157 ± 7	23.7 ± 0.7	− 10.2 ± 0.4	− 17.0 ± 0.5
170	149 ± 7	191 ± 8	145 ± 6	23.4 ± 0.7	− 10.5 ± 0.4	− 17.0 ± 0.5
180	133 ± 7	178 ± 8	133 ± 6	22.7 ± 0.7	− 11.1 ± 0.4	− 17.0 ± 0.5
190	119 ± 6	165 ± 8	121 ± 5	22.2 ± 0.7	− 11.6 ± 0.4	− 16.9 ± 0.5
200	106 ± 5	154 ± 8	111 ± 5	21.7 ± 0.7	− 12.0 ± 0.4	− 16.8 ± 0.5
210	90 ± 4	138 ± 8	96 ± 4	21.2 ± 0.7	− 12.3 ± 0.4	− 16.7 ± 0.5
220	81 ± 4	132 ± 7	92 ± 4	20.5 ± 0.7	− 13.0 ± 0.4	− 16.8 ± 0.5
230	68 ± 4	122 ± 7	83 ± 4	19.9 ± 0.7	− 13.6 ± 0.4	− 16.7 ± 0.5
240	58 ± 3	115 ± 7	76 ± 4	19.2 ± 0.7	− 14.1 ± 0.4	− 16.7 ± 0.5
250	47 ± 3	106 ± 6	69 ± 3	18.7 ± 0.7	− 14.6 ± 0.4	− 16.7 ± 0.5
260	39 ± 2	98 ± 5	62 ± 3	18.3 ± 0.7	− 14.9 ± 0.4	− 16.6 ± 0.5
270	31 ± 2	93 ± 5	57 ± 3	17.7 ± 0.7	− 15.4 ± 0.4	− 16.5 ± 0.5
280	20 ± 2	84 ± 4	51 ± 3	16.7 ± 0.7	− 16.1 ± 0.4	− 16.4 ± 0.5
290	10 ± 1	76 ± 3	44 ± 2	16.5 ± 0.7	− 16.5 ± 0.4	− 16.5 ± 0.5
293	8.3 ± 0.5	74 ± 3	42 ± 2	16.5 ± 0.7	− 16.5 ± 0.4	− 16.5 ± 0.5
300	8.6 ± 0.5	74 ± 3	41 ± 2	16.5 ± 0.7	− 16.5 ± 0.4	− 16.5 ± 0.5
310	8.8 ± 0.5	75 ± 3	42 ± 2	16.5 ± 0.7	− 16.4 ± 0.4	− 16.5 ± 0.5
320	9.1 ± 0.5	75 ± 3	42 ± 2	16.6 ± 0.7	− 16.4 ± 0.4	− 16.5 ± 0.5
330	9.2 ± 0.5	75 ± 3	42 ± 2	16.6 ± 0.7	− 16.4 ± 0.4	− 16.5 ± 0.5
340	9.6 ± 0.5	75 ± 3	42 ± 2	16.7 ± 0.7	− 16.4 ± 0.4	− 16.5 ± 0.5
350	9.5 ± 0.5	75 ± 3	41 ± 2	16.7 ± 0.7	− 16.3 ± 0.4	− 16.5 ± 0.5
360	9.4 ± 0.5	75 ± 3	41 ± 2	16.8 ± 0.7	− 16.3 ± 0.4	− 16.6 ± 0.5
370	9.1 ± 0.5	74 ± 3	40 ± 2	16.9 ± 0.7	− 16.3 ± 0.4	− 16.6 ± 0.5
380	8.6 ± 0.4	74 ± 3	39 ± 2	16.9 ± 0.7	− 16.2 ± 0.4	− 16.6 ± 0.5
390	7.6 ± 0.4	72 ± 3	38 ± 2	17.0 ± 0.7	− 16.2 ± 0.4	− 16.6 ± 0.5
400	6.5 ± 0.3	71 ± 3	37 ± 2	17.1 ± 0.7	− 16.2 ± 0.4	− 16.6 ± 0.5

are almost independent of temperature for both the $(Eu_2O_3)_{0.186}(P_2O_5)_{0.814}$ glass (Table IV) and the $(Eu_2O_3)_{0.20}(P_2O_5)_{0.80}$ glass (Table V): the vibrational anharmonicities do not change much at higher temperatures.

The measurements made down to 77 K of the TOEC for both the $(Eu_2O_3)_{0.186}(P_2O_5)_{0.814}$ glass (Table VII) and $(Eu_2O_3)_{0.20}(P_2O_5)_{0.80}$ glass (Fig. 9) enable determination of the temperature dependences of γ_L and γ_S (Tables IV and V). These are particularly instructive. As the temperature is reduced the magnitude of γ_L becomes much greater: the longitudinal acoustic mode softening becomes more enhanced at low temperatures. The shear mode, γ_S, does get bigger but not to the same extent. Similar behaviour has been found for samarium phosphate glasses [13]. Vitreous SiO_2 has positive TOEC (except the smallest C_{456}) which increase as the temperature is reduced from 293 K to 77 K, and negative acoustic mode Grüneisen parameters, γ_L and γ_S, the former being the larger, both increasing as the temperature decreases [18]. This unusual vibrational anharmonicity of the long-wavelength acoustic modes is not a general characteristic of amorphous materials: vitreous TeO_2, the only glass with more normal elastic properties whose non-linear elastic properties have yet been studied as a function of temperature, has negative TOEC and its γ_L and γ_S are positive and do not vary much with temperature [35].

The physical origin of the anomalous negative values obtained for the hydrostatic pressure derivatives $(\partial C_{11}/\partial P)_{T,P=0}$ and $(\partial C_{44}/\partial P)_{T,P=0}$ of the elastic stiffnesses and $(\partial B/\partial P)_{T,P=0}$ of the bulk modulus and the positive values for the corresponding TOEC combinations and the negative acoustic mode Grüneisen parameters, γ_L and γ_S, of the europium and samarium phosphate glasses and vitreous SiO_2 remains uncertain. Both the rare-earth elements europium and samarium can show pressure-varying, volume-sensitive, mixed valence – a possible explanation [7, 8, 13]. However, the present laser fluorescence studies were unable to establish the presence of divalent europium ion in sufficient quantities to produce the observed large elastic anomalies. This is also the case in the samarium phosphate glasses [14]. Mixed valence is not the cause of the anomalous vibrational anharmonicity.

Glasses seem to include three groups of excess excitations in addition to sound waves: (i) harmonic modes in the range 200 GHz–1 THz; (ii) a relaxation contribution to the excitation spectrum; (iii) tunnelling or two level states [46]. There is evidence to support [46] a common interpretation [47] of these low-frequency excitations in vitreous SiO_2 in terms of ther-

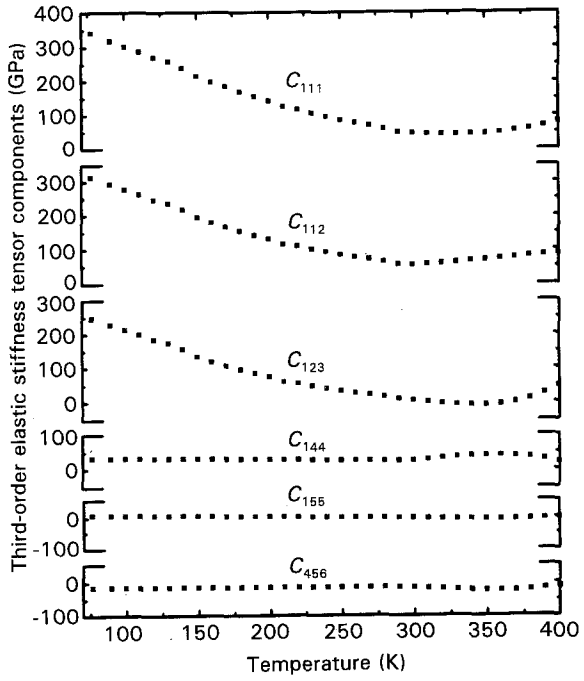

Figure 9 The temperature dependences of the third-order elastic stiffness tensor components C_{IJK} for $(Eu_2O_3)_{0.20}(P_2O_5)_{0.80}$ glass.

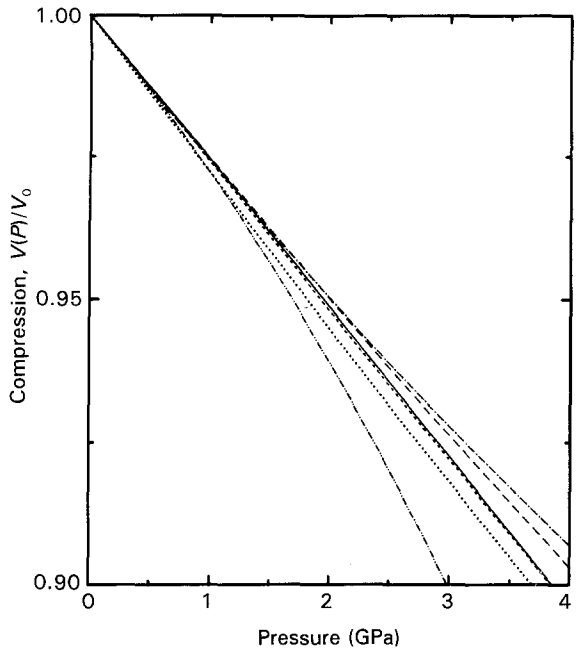

Figure 10 The compression $V(P)/V_0$ of (——) $(Eu_2O_3)_{0.186}(P_2O_5)_{0.814}$ and (- - -) $(Eu_2O_3)_{0.20}(P_2O_5)_{0.80}$ glasses at 293 K extrapolated to high pressure compared with those of (···) $(Sm_2O_3)_{0.212}(P_2O_5)_{0.788}$, (---) $(Sm_2O_3)_{0.248}(P_2O_5)_{0.752}$, (-·-) $(Nd_2O_3)_{0.235}(P_2O_5)_{0.765}$ glasses and (-···-) vitreous SiO_2.

mally activated relaxation processes. A characteristic feature of many vitreous materials is a broad peak in the ultrasonic attenuation as a function of temperature considered to be due to excitations arising from thermally activated motions of relaxing "particles" over potential barriers. The europium phosphate glasses show this acoustic attenuation peak above 20 K.

In the case of vitreous SiO_2 the pressure-induced, acoustic-mode softening effects have been attributed to non-linear acoustic contributions from bending vibrations of the bridging oxygen atoms which correspond to transverse motion against small force constants and are allowed in the open structure based on SiO_4 tetrahedra [48, 49]. Another possible source is rotations of coupled SiO_4 tetrahedra involved in low-frequency harmonic vibrations [46, 50]. Similar non-linear effects in vibrational modes associated with the corner-linked PO_4 tetrahedra, which constitute the structure, could be responsible for the elastic anomalies of the phosphate glasses. Thus, either bending vibrations of the bridging oxygen ions or rotations of coupled PO_4 tetrahedra could be the origin of the acoustic-mode softening under pressure. There is a difficulty with this explanation. Phosphate glasses containing lanthanum [8, 9], neodymium [12, 41, 42], iron [39] and molybdenum [40] show positive values for the hydrostatic pressure derivatives $(\partial C_{11}/\partial P)_{T,P=0}$ and $(\partial C_{44}/\partial P)_{T,P=0}$ of the elastic stiffnesses and $(\partial B/\partial P)_{T,P=0}$ of the bulk modulus. It is plausible that the anomalous elastic behaviour under pressure of the vitreous europium and samarium phosphates could result from previously unrecognized subtle structural features different from those of the other phosphate glasses, which have been studied to date. The present observation that the fluorescence of the europium phosphate glasses is consistent with presence of two distinct sites close in energy for the Eu^{3+} ions is in line with this suggestion. These sites could comprise the double well system required to explain the elastic and inelastic properties of these glasses. Resolution of the problem of whether the origin of these effects is associated with a structural feature must await the results of further experimental studies, now in progress, of the effects of pressure on the elastic behaviour of other rare-earth phosphate glasses.

Acknowledgements

We thank the Johnson Matthey Technology Centre (Dr S. Bartlett) and DRA Maritime Division (S. Takel) for support of our programme of work on rare-earth oxide glasses. E. F. Lambson, D. Perry, School of Pharmacy and Pharmacology, H. Perrott and Dr G. Love, Centre for Electron Optical Studies, are thanked for technical assistance and Professor G. Carini, University of Messina, for many useful discussions. H.B.S. is grateful to the University Pertanian Malaysia and the Government of Malaysia for financial support.

References

1. F. M. DURVILLE, E. G. BEHRENS and R. C. POWELL, *Phys. Rev. B* **34** (1986) 4213.
2. E. G. BEHRENS, F. M. DURVILLE and R. C. POWELL, *Opt. Lett.* **11** (1986) 653.
3. E. G. BEHRENS, F. M. DURVILLE, R. C. POWELL and D. H. BLACKBURN, *Phys. Rev. B* **39** (1989) 6076.
4. E. G. BEHRENS, R. C. POWELL, and D. H. BLACKBURN, *J. Opt. Soc. Am. B* **7** (1990) 1437.
5. V. A. FRENCH, R. C. POWELL, D. H. BLACKBURN and D. C. CRANMER, *J. Appl. Phys.* **69** (1991) 913.

6. M. M. BROER, A. J. BRUCE and W. H. GRODKIEWICZ, *Phys. Rev. B* **45** (1992) 7077.
7. A. MIERZEJEWSKI, G. A. SAUNDERS, H. A. A. SIDEK and B. BRIDGE, *J. Non-Cryst. Solids* **104** (1988) 323.
8. A. MIERZEJEWSKI, G. A. SAUNDERS, H. A. A.SIDEK, R. N. HAMPTON and I. J. AL-MUMMAR, *Solid State Ionics* **28–30** (1988) 778.
9. H. A. A. SIDEK, G. A. SAUNDERS, R. N. HAMPTON, R. C. J. DRAPER and B. BRIDGE, *Philos. Mag. Lett.* **57** (1988) 53.
10. QINGXIAN WANG, G. A. SAUNDERS, E. F. LAMBSON, V. BAYOT and J.-P. MICHENAUD, *J. Non-Cryst. Solids* **125** (1990) 287.
11. G. CARINI, M. CUTRONI, G. D'ANGELO, M. FEDERICO, G. GALLI, G. TRIPODO, G. A. SAUNDERS and Q. WANG, *ibid.* **121** (1990) 288.
12. H. B. SENIN, Q. WANG, G. A. SAUNDERS, R. C. J. DRAPER, H. M. FAROK, M. CANKURTARAN, P. J. FORD, W. POON, H. VASS and B. BRIDGE, in "Developments in Acoustics and Ulrasonics", edited by M. Povey and J. McClements (Institute of Physics, London, 1992) p. 197.
13. H. B. SENIN, Q. WANG, G. A. SAUNDERS and E. F. LAMBSON, *J. Non-Cryst. Solids* **152** (1993) 83.
14. H. M. FAROK, G. A. SAUNDERS, W. POON and H. VASS, *ibid.* **142** (1992) 175.
15. S. FREED and S. KATCOFF, *Physica* **14** (1948) 17.
16. V. N. BAPAT, *J. Phys. C Solid State Phys.* **10** (1977) L465.
17. E. P. PAPADAKIS, *J. Acoust. Soc. Am.* **42** (1967) 1045.
18. Q. WANG, G. A. SAUNDERS, H. B. SENIN and E. F. LAMBSON, *J. Non-Cryst. Solids* **143** (1992) 65.
19. Y. K. YOGURTCU, E. F. LAMBSON, A. J. MILLER and G. A. SAUNDERS, *Ultrasonics* **18** (1980) 155.
20. R. N. THURSTON and K. BRUGGER, *Phys. Rev. A* **133** (1964) 1604.
21. J. A. CAPOBIANCO, P. P. PROULX, M. BETTINELLI and F. NEGRISOLO, *Phys. Rev. B* **42** (1990) 5936.
22. D. S. McCLURE and Z. KISS, *J. Chem. Phys.* **39** (1963) 3251.
23. L. G. DeSHAZER and G. H. DIEKE, *ibid.* **38** (1963) 2190.
24. C. BRECHER, *ibid.* **61** (1974) 2297.
25. W. A. RUNCIMAN, *Rept. Progr. Phys.* **21** (1958) 30.
26. V. S. KISHAN KUMAR, S. B. S. SASTRY and B. S. V. S. R. ACHARYULU, *Phys. Status Solidi B* **155** (1989) 679.
27. S. W. MARTIN, *Eur. J. Solid State Inorg. Chem.* **28** (1991) 163.
28. J. R. VAN WAZER and D. A. CAMPANELLA, *J. Am. Chem. Soc.* **72** (1950) 655.
29. V. FAWCETT, D. A. LONG and L. H. TAYLOR, in "Proceedings of the 5th International Conference on Raman Spectroscopy" (Freiburg, 1976) p.112.
30. G. K. SHIH and G. J. SU, *Compt. Rend.* **48**, 7th Cong. Int. Verre, Bruxelles (1965).
31. D. W. HALL, S. A. BRAWER and M. J. WEBER, *Phys. Rev.* **B25** (1982) 2828.
32. L. PICHE, R. MAYNARD, S. HUNKLINGER and J. JÄCKLE, *Phys. Rev. Lett.* **32** (1974) 1426.
33. S. HUNKLINGER, *J. Phys. Paris* **43** (1982) C9-461.
34. A. K. RAYCHAUDHURI and S. HUNKLINGER, *Z. Phys.* **B57** (1984) 113.
35. N. BENBATTOUCHE, G. A. SAUNDERS and H. A. A. SIDEK, *Philos. Mag. B* **60** (1989) 643.
36. M. P. BRASSINGTON, W. A. LAMBSON, A. J. MILLER, G. A. SAUNDERS and Y. K. YOGURTCU, *ibid.* **42** (1980) 127.
37. M. P. BRASSINGTON, A. J. MILLER and G. A. SAUNDERS, *ibid.* **43** (1981) 1049.
38. M. P. BRASSINGTON, TU HAILING, A. J. MILLER and G. A. SAUNDERS, *Mater. Res. Bull.* **16** (1981) 613.
39. M. P. BRASSINGTON, A. J. MILLER, J. PELZL and G. A. SAUNDERS, *J. Non-Cryst. Solids* **44** (1981) 157.
40. J. D. COMINS, J. E. MACDONALD, E. F. LAMBSON, G. A. SAUNDERS, A. J. ROWELL and B. BRIDGE, *J. Mater. Sci.* **22** (1987) 2113.
41. H. B. SENIN, H. A. A. SIDEK, P. J. FORD, G. A. SAUNDERS, Q. WANG, R. C. J. DRAPER and W. A. LAMBSON, in "Advances in Amorphous State Chemistry" (Society of Glass Technology, Sheffield, 1993) p. 55.
42. H. A. A. SIDEK, H. B. SENIN, G. A. SAUNDERS and P. J. FORD (J. Fizik, Malaysia) in press.
43. E. H. BOGARDUS, *J. Appl. Phys.* **36** (1965) 2504.
44. F. D. MURNAGHAN, *Proc. Natn Acad. Sci.* **30** (1944) 244.
45. O. L. ANDERSON, *J. Phys. Chem. Solids* **27** (1966) 547.
46. U. BUCHENAU, H. M. ZHOU, N. NUCKER, K. S. GILROY and W. A. PHILLIPS, *Phys. Rev. Lett.* **60** (1988) 1318.
47. F. N. IGNATIEV, V. G. KARPOV and M. I. KLINGER, *J. Non-Cryst. Solids* **55** (1983) 307.
48. Y. SATO and O. L. ANDERSON, *J. Phys. Chem. Solids* **41** (1980) 401.
49. E. F. LAMBSON, G. A. SAUNDERS, B. BRIDGE and R. A. El-MALLAWANY, *J. Non-Cryst. Solids* **69** (1984) 117.
50. L. GUTTMANN and S. H. RAHMAN, *Phys. Rev. B* **33** (1986) 1506.

Received 22 October 1993
and accepted 6 January 1994